Int. J. Electrochem. Sci., 14 **(2019)** 7961 – 7972, doi: 10.20964/2019.08.06

International Journal of ELECTROCHEMICAL SCIENCE
www.electrochemsci.org

Construction of Highly Active Pt/Ni-Fe Layered Double Hydroxide Electrocatalyst towards Methanol Oxidation in Alkaline Medium

Haiyan Wang[1], Yanan Chen[1], Wenfu Xie[1], Xiaoxue Han[1], Qian Feng[1], Rong Jiang[1], Hu Shang[1], Feifei Zhang[,1], Linna Gao[2], Zonghua Wang[1]*

[1] College of Chemistry and Chemical Engineering, Shandong Sino-Japanese Center for Collaborative Research of Carbon Nanomaterials, Qingdao University, Qingdao 266071, China
[2] College of Chemical and Environmental Engineering, Shandong University of Science and Technology, Qingdao, 266590, China
[*]E-mail: zhangfeifei00921@163.com

Received: 20 March 2019 / *Accepted:* 15 May 2019 / *Published:* 30 June 2019

A novel Pt/Ni-Fe layered double hydroxide (Pt/Ni-Fe LDH) electrocatalyst was fabricated by a two-step facile process for oxidation of methanol in alkaline medium. It is found that Pt/Ni-Fe LDH electrocatalyst exhibits higher electrocatalytic activity, better anti-poisoning ability and stability for methanol oxidation comparing to pure Pt black and commercial Pt/C catalyst. Such an enhancement is probably attributed to the synergistic effect of Ni-Fe LDH and the uniform loading of Pt nanoparticles on the LDH layers. When ionic liquid (IL) was introduced to the composites, the prepared Pt/IL/Ni-Fe LDH exhibits even better electrocatalytic behaviors (205.6 mA mg^{-1}_{Pt}, I_f/I_b=5.67) than the Pt/Ni-Fe LDH. Moreover, the morphology and structure of composites were characterized using scanning electron microscope equipped with an energy dispersive X-ray spectrometry, transmission electron microscope, X-ray diffraction, and FT-IR spectra. It is found that the Ni-Fe LDH have a flake-like morphology, the mean diameter of Pt nanoparticles in Pt/Ni-Fe LDH and Pt/IL/Ni-Fe LDH electrocatalyst is 4.36 nm and 3.09 nm, smaller than that in pure Pt black and commercial Pt/C electrocatalyst (8.70 nm and 6.48 nm).

Keywords: Electrocatalyst, Methanol oxidation, Ionic liquid, Pt/Ni-Fe layered double hydroxide

1. INTRODUCTION

Direct methanol fuel cells (DMFCs) are considered as one of the most prospective power supplies for portable electronic devices, automobiles, and distributed stationary power sources by virtue of their higher energy-conversion efficiency, simple mechanism, clean and no pollution [1, 2]. At the present stage, most of the commercial DMFCs are employed Pt black and Pt/C as anode catalyst to oxidize methanol [3, 4]. However, Pt black and Pt/C catalyst suffers from the scarcity and high cost [5].

Moreover, the methanol oxidation reaction (MOR) is a very complex reaction process, during which much incomplete oxidation intermediate product such as carbon monoxide (CO) are generated and enriched[6, 7]. The intermediate species could absorb the reaction active sites on Pt surface, suppress the adsorption-oxidation of methanol [8]. Many supporting materials with high specific surface area, good electric conductivity, and electrochemical stability have been employed to improve the composites catalytic effect and stability, such as nano-carbon materials[9, 10], metal oxides[11, 12] and hybrid materials[13, 14].

Layered Double Hydroxides (LDHs), are a class of important lamellar materials[15]. They have chemical composition described as the general formula: $[M^{II}_{1-x}M^{III}_{x}(OH)_2]^{x+}$ $[A^{n-}]_{x/n}\cdot yH_2O$, where M^{II} and M^{III} are arranged as divalent and trivalent metal cations in the LDHs layers, A^{n-} is an *n*-valent anion, and *y* is the number of interlayer water molecules[16]. The isomorphous substitution in divalent metal cations by the trivalent one's results in a positive charge, which is compensated by interlayer anions [17]. In the last ten years, LDHs have been applied in numerous fields of supercapacitors, biosensors, fuel cells and other fields on account of their attractive properties including well anion-exchange ability, high surface area, low cost, good catalytic activity and stability[18, 19].

In a recent work, the Pd/LDH-NWs composite was synthesized by an in situ redox reaction with Pd nanoparticles uniformly loading on the Co-Al LDH nanowalls. The Pd/LDH-NWs composite shown better catalytic activity and stability for ethanol oxidation than Pd/C catalyst [20]. Due to the specific layered structure and high specific surface area, a Ni-Fe LDH based catalyst was also reported for oxygen evolution reaction with fast diffusion rate for the reactant and product[21]. The application of LDHs in catalytic oxidation of methanol is restricted due to its poor electrical conductivity. In order to improve the electrical conductivity, several substances have been introduced to LDH materials, for example, carbon quantum dots, carbon nanotube and graphene [22-24]. Recently, ionic liquids (ILs) have been used in multidisciplinary areas by virtue of their specific characteristics, such as high ionic conductivity, good solubility, and good electrochemical stability [25]. The previous report indicated that Pt and Pt alloy NPs could uniformly load on ILs modified carbon nanotubes, which showed good performance in the electrooxidation of methanol [26]. Recently, an ILs functionalized MgAl-LDH was synthesized and used for the immobilization of myoglobin. The obtained hybrid showed good electrocatalytic activity, lower detection limit and better stability for methanol oxidation. In other words, ILs exhibit good ionic conductivity, which could increase the loading of Pt NPs on supporting materials and improve the conductivity of LDHs [27].

In this work, the novel Pt/Ni-Fe LDH and 1-butyl-3- methylimidazolium tetrafluoroborate (*Ionic Liquid,* IL) functionalized Pt/Ni-Fe LDH (Pt/IL/Ni-Fe LDH) electrocatalyst is firstly synthesized by a two-step facile process. The key aspects of this electrocatalyst are the formation of ultrathin Ni-Fe LDH nanoplates and association with the uniform loading of Pt NPs (The schematic model was shown in Figure 1). The prepared Pt/IL/Ni-Fe LDH electrocatalyst displayed excellent electrocatalytic activity with a high peak current density and also good stability for methanol oxidation.

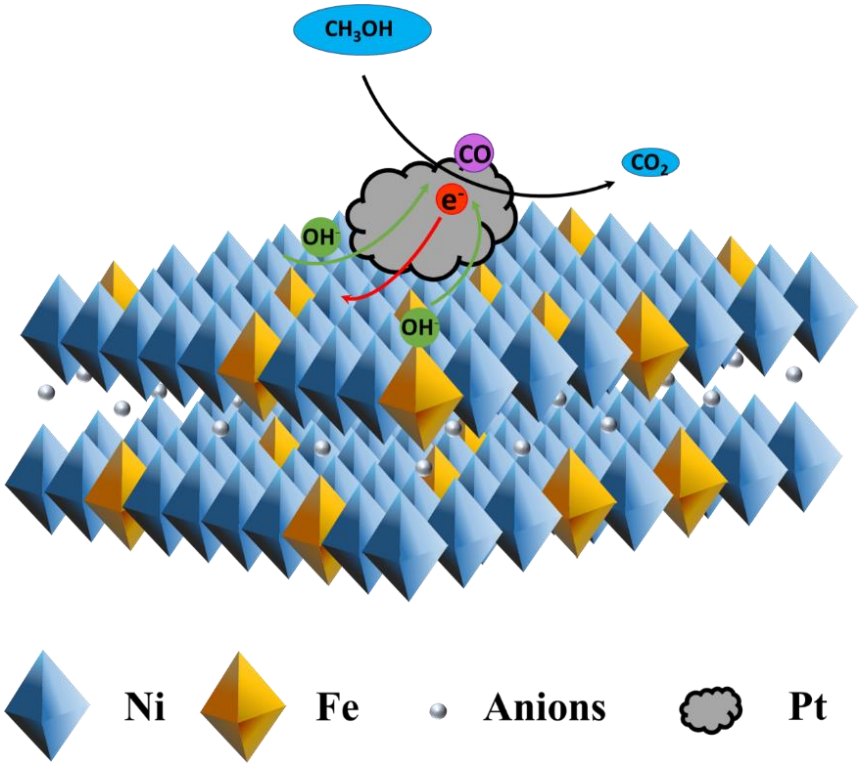

Figure 1. Schematic model of the roles of Pt/Ni-Fe LDH elecotrocatalyst for methanol electrooxidation.

2. EXPERIMENTS

2.1. Materials

1-butyl-3-methylimidazolium tetrafluoroborate ([bmim][BF_4]) was purchased from Lanzhou Institute of Chemical Physics, Chinese Academy of Sciences. $H_2PtCl_6 \cdot 6H_2O$, Pt black, commercial Pt/C catalyst (containing 20 wt% Pt), NaOH, $Ni(NO_3)_2 \cdot 6H_2O$, $Fe(NO_3)_3 \cdot 9H_2O$, anhydrous N, N-dimethylformamide (DMF) and methanol were purchased from Aladdin Chemistry Co. Ltd. All reagents were used as received.

2.2. Instrumentation

The SEM images were obtained by scanning electron microscope (JEOL JSM-6700F) with an energy dispersive X-ray spectrometry (EDS). TEM images and selected-area electron diffraction (SAED) pattern were performed using a JEOL JEM-2100 system, at an operating votage of 200 kV. X-ray diffraction were taken on a DX-2700 (Haoyuan, China) powder X-ray diffraction (XRD, Cu-Kα radiation λ=0.15418 nm). FT-IR spectra were performed on a Nicolet-5700 spectrophotometer (Madison, USA). The electrochemical tests of the electrocatalyst were conducted on a CHI 660B electrochemical workstation equipped with a three-electrode system. A platinum wire was used as the counter electrode; saturated calomel electrode (SCE) and glassy carbon electrode (GCE) was used as the reference and the working electrode, respectively. For more information about the setting parameters in electrochemical tests are given in the corresponding results part.

2.3. Synthesis of Ni-Fe LDH

In a typical synthesis [28], 139.8 mg of nickel nitrate hexahydrate and 39.0 mg of iron nitrate nonahydrate (with a molar ratio of Ni/Fe = 5) were dispersed in 24 mL of DMF. The solution was thoroughly and constantly stirred at 85°C for 4 h. After that, a 100 ml stainless steel with Teflon liner was charged with the above solution, 48 ml water and 24 ml DMF with constant vigorous magnetic stirring. The vessel was then sealed, heated to 120°C and remained to react for 12 h, and followed at 160°C for 2 h. The product was gathered by centrifuge and washed with water.

2.4. Preparation of Ni-Fe LDH and Pt/IL/Ni-Fe LDH electrocatalyst

The electrocatalysts were synthesized by the following process, 100 mg of Ni-Fe LDH was added into 30 mL doubly distilled water and supersonic treated for 15 min, followed by the addition of 30 mg [bmim][BF_4] ionic liquid (IL). Then 2.5 mL of 77 mM H_2PtCl_6 was added into above suspensions under vigorous stirring. Afterward, excess amount of 100 mM sodium borohydride ($NaBH_4$) alkaline solution was added cautiously, followed by vigorously stirring for 24 h. Finally, the suspension was washed with doubly distilled water, and the resulting solids were dried at 50°C for 24 h. The as-prepared electrocatalyst was denoted as Pt/IL/Ni-Fe LDH. The theoretical content of Pt is 28.8 wt%. As controls, Pt, Pt/Ni-Fe LDH electrocatalyst was also synthesized by the same procedures except for without Ni-Fe LDH and ionic liquid, respectively.

20 mg of each electrocatalyst was ultrasonically dispersed in 20 ml doubly distilled water for 15 min. Then 6 μl of as-prepared solution was pipetted onto the well-polished GCE and dried at room temperature.

3. RESULTS AND DISCUSSION

The morphology and nanostructure of Ni-Fe LDH were examined by the SEM and TEM at different magnifications (Figure 2). It can be observed that the Ni-Fe LDH have a flake-like morphology. The thicknesses and lateral sizes of the LDHs are in a range of 10-20 nm and 150-600 nm, respectively. The selected-area electron diffraction (SAED) pattern of the nano-flake reveals hexagonally arrange bright spots (insert of Figure 2C), confirming the single-crystal nature of as-obtained Ni-Fe LDH and suggesting its relatively good electron transportation ability. The layered and open structure is benefit to support the NPs. XRD pattern of Ni-Fe LDH indicated by the diamonds are shown in figure 4B-a, the diffraction peaks at 2θ = 12.1°, 22.5°, 35.6°, 42.7°, 59.1° and 62.3°are attributed to the (003), (006), (009), (018), (110) and (113) diffraction peaks, which is in accordance with that reported in the earlier literatures [29-31]. The FT-IR spectra of the Ni-Fe LDH and Pt/Ni-Fe LDH, ranging from 4000 to 40 cm^{-1}, are illustrated in figure 4A.

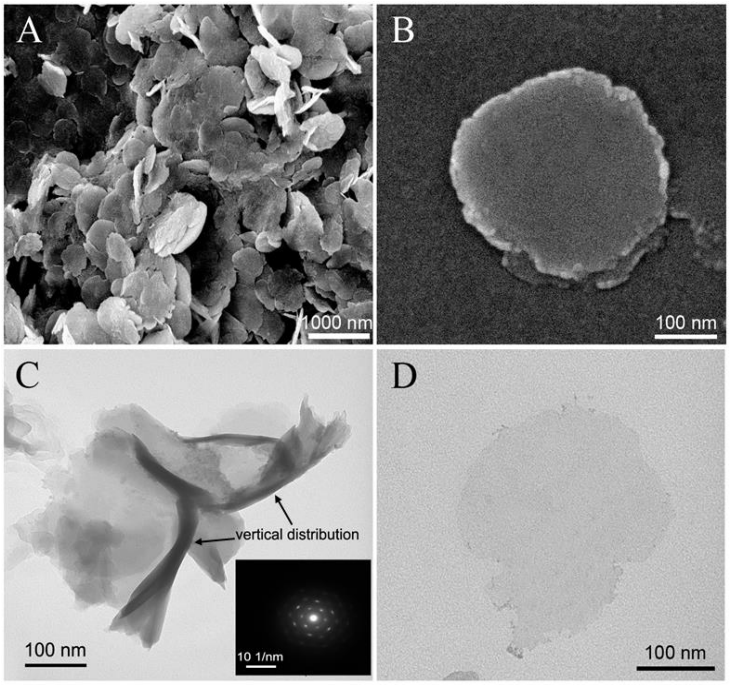

Figure 2. SEM (A and B) and TEM (C and D) images of the Ni-Fe LDH at different magnifications.

The broad band appeared around 3467 cm^{-1} is related to the hydroxyl stretching band of metal-hydroxyl groups and hydrogen-bonded interlayer of water molecules[32]. The absorption at 1650 cm^{-1} is related to the bending vibration of water [33]. Nitrate anion gives a very strong absorption peak at 1388 cm^{-1} [34]. The broad band at 595 cm^{-1} is related to the bending vibration of metal-oxygen [20].

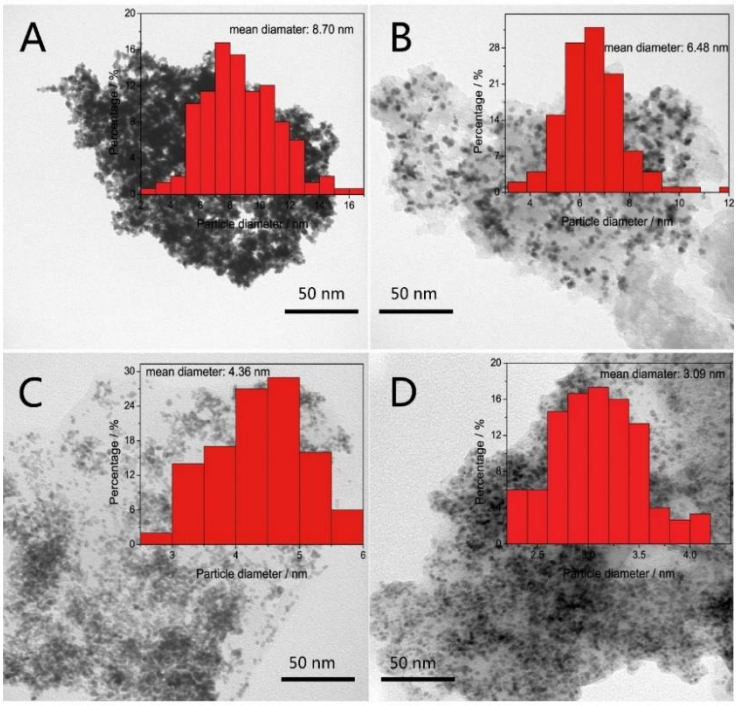

Figure 3. TEM images and histograms of particle size distribution (inset figure) of Pt black (A), Pt/C (B), Pt/Ni-Fe LDH (C) and Pt/IL/Ni-Fe LDH (D).

Figure 3 shows the TEM images of Pt black (A), commercial Pt/C (B), Pt/Ni-Fe LDH (C) and Pt/IL/Ni-Fe LDH (D), and corresponding histograms of particle size distribution (inset figures). For each sample, 200 randomly chosen particles were chosen from TEM images for calculating the mean diameter of Pt NPs.

It can be seen that as-prepared Pt black electrocatalyst with a mean diameter of 8.70 nm was dispersed unevenly without the support materials, and the purchased commercial Pt/C electrocatalyst displayed a large mean diameter (6.48 nm). Notably, the Pt NPs loading on Ni-Fe LDH nano-flakes showed the better uniformity and smaller particle size (4.36 nm), indicating that Ni-Fe LDH nano-flakes make a real difference in dispersing the NPs here. The uniform distribution may be attributed to the high surface area of Ni-Fe LDH nano-flakes, which could supply more sites for the effective reduction adsorption, and inhibit the aggregation of the NPs. More interestingly, at the regulation of IL, Pt NPs could disperse homogeneously even more (3.09 nm). That is because IL could influence the dispersion of $PtCl_6^{2-}$, and then prevent Pt particles from being uniting at the same site during the reduction reaction [35].

The XRD patterns of the Pt black and Pt/Ni-Fe LDH electrocatalyst are presented in Figure 4B. For Pt black electrocatalyst (Figure 4B-b), the diffraction peaks indicated by the clubs at 2θ values of about 41.2°, 46.2°, 66.6° and 81.3° corresponding to (111), (200), (220) and (311) planes of a pure face-centered cubic structure of Pt [36]. Compared to the XRD pattern of Pt, extra diffraction peaks (Figure 4B-C) appear at the 2θ values of about 12.5°, 22.3° and 33.6° can be assigned to the (003), (006) and (009) diffractions of Ni-Fe LDH, suggesting the formation of the Pt/Ni-Fe LDH electrocatalyst. Furthermore, EDS spectra (Figure 4C) confirms that the Ni-Fe LDH was synthesized successfully and the Pt NPs (Pt content of 17.7%) was loaded effectively. The atomic ratio of Ni and Fe in Ni-Fe LDH was estimated ~ 4.7.

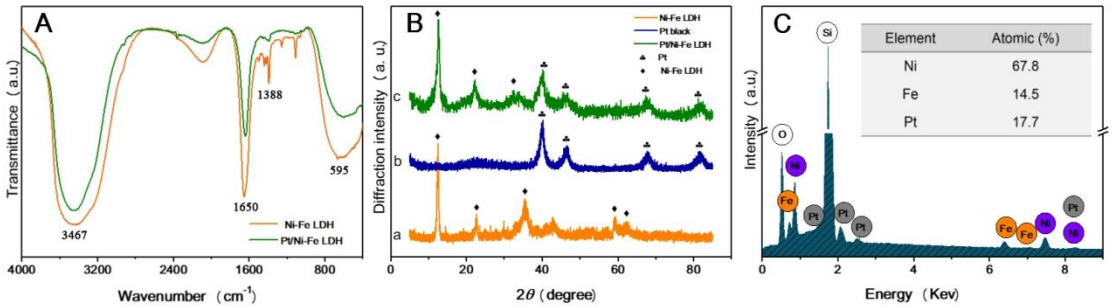

Figure 4. FT-IR spectra (A) of Ni-Fe LDH and Pt/Ni-Fe LDH, XRD patterns (B) of Ni-Fe LDH (a), Pt black (b) and Pt/Ni-Fe LDH (c). The EDS spectra (C) of Pt/Ni-Fe LDH.

The electrochemically active surface area (ECSA) was measured by using cyclic voltammetry (CV) method. Figure 5 shows the typical CVs recorded of the Pt black, commercial Pt/C, Pt/Ni-Fe LDH, and Pt/IL/Ni-Fe LDH electrocatalyst in nitrogen-saturated 1.0 M NaOH solution at a scan rate of 100 mV s^{-1} with the potential between -1.0 and 0.2 V vs. SCE. The ECSA of electrocatalysts were calculated based on the following equation (1)[37].

$$ECSA = Q_H / (C \times m) \quad (1)$$

Where Q_H is the integrated charge for H-desorption between -1.0 and -0.6 V, C is the charge required for the monolayer adsorption of hydrogen on Pt surface (210 μC cm^{-2}), m is the mass of Pt loading on the GCE. The ECSA value (Table 1) of Pt/IL/Ni-Fe LDH (203.9 cm^2 mg^{-1}_{Pt}) is higher than those of Pt black (124.8 cm^2 mg^{-1}_{Pt}), commercial Pt/C (147.1 cm^2 mg^{-1}_{Pt}) and Pt/Ni-Fe LDH (153.7 cm^2 mg^{-1}_{Pt}), that may be caused by the smaller size and much better dispersion of Pt NPs on the Ni-Fe LDH. This result also reveals that the electrocatalytic reactions occur more accessible and much easier on the Pt/IL/Ni-Fe LDH[7].

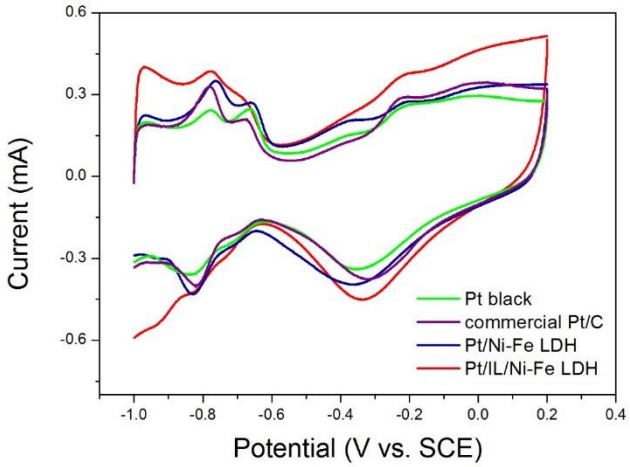

Figure 5. CVs of Pt black, commercial Pt/C, Pt/Ni-Fe LDH and Pt/IL/Ni-Fe LDH electrocatalyst in 1.0 M NaOH at 100 mV s^{-1}.

CV scanning was used to study the electrochemical oxidation of methanol on the electrocatalyst. Figure 6 shows the typical CVs recorded in 1.0 M CH_3OH containing 1.0 M NaOH at a scan rate of 100 mV s^{-1}. As we can see from the figure, the Ni-Fe LDH yields negligible current under identical measurements in comparison to the other three electrocatalysts. Therefore, we will focus on the catalytic ability difference of Pt black, commercial Pt/C, Pt/Ni-Fe LDH and Pt/IL/Ni-Fe LDH electrocatalyst later (Table 1). Two anodic peaks can be obviously observed in the CV record, one at about -0.26 V in the forward scan, which is ascribed to the oxidation of methanol to CO_2 and other carbonaceous species, such as CO[5]. Another one at about -0.4 V in the reverse scan is ascribed to the oxidized removal of the CO and other carbonaceous species generated in the forward scan [5]. The peak current density in the forward scan for Pt/Ni-Fe LDH is 119.2 mA mg^{-1}_{Pt}, which is higher than that of Pt black (83.6 mA mg^{-1}_{Pt}) and commercial Pt/C (107.3 mA mg^{-1}_{Pt}), suggesting the Ni-Fe LDH can promote the electrocatalytic ability of Pt on methanol oxidation. The layered structure of Ni-Fe LDH could provide more locations for the Pt formation and thus inhibit the aggregation of Pt particles [28]. The smaller the particle size, the greater the specific surface area, and thus more active sites are exposed, which would be beneficial to electrochemical reaction [7].

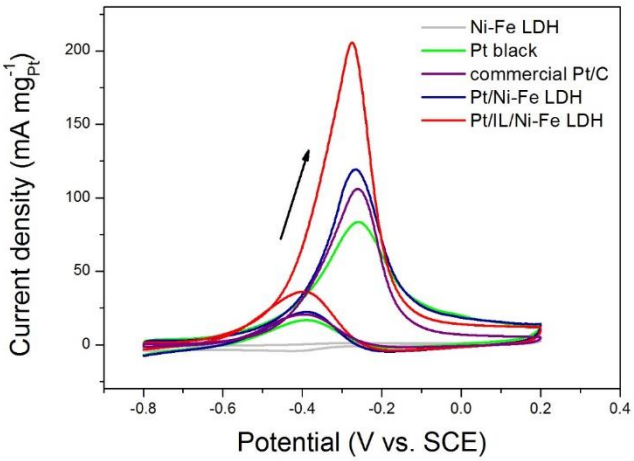

Figure 6. CVs of Ni-Fe LDH, Pt black, commercial Pt/C, Pt/Ni-Fe LDH and Pt/IL/Ni-Fe LDH electrocatalyst in 1.0 M CH_3OH solution containing 1.0 M NaOH at 100 mV s^{-1}.

The peak current density in the forward scan for Pt/IL/Ni-Fe LDH is 205.6 mA mg^{-1}_{Pt}, which 1.7 times higher than that of Pt/Ni-Fe LDH. On the one hand, IL can increase the material's conductivity that will accelerate electron transport. On the other hand, IL could influence the dispersion of $PtCl_6^{2-}$, preventing Pt particles from being uniting at the same site, reducing particle size.

In addition, the ratio of forward-to-backward oxidation current, I_f/I_b, is an important parameter of the electrocatalyst tolerance to CO and other poisoning carbonaceous species [38]. A higher value demonstrates that the oxidation removal of the poisoning carbonaceous species on the electrocatalyst surface is much easier. As calculated, the I_f/I_b ratio of Pt/IL/Ni-Fe LDH is 5.67, which is higher than those of the Pt black (4.98), commercial Pt/C (5.09) and Pt/Ni-Fe LDH catalysts (5.32), showing better anti-poisoning ability. Several reported works have been listed in Table 1 for comparison. As we can see, the synthesized electrocatalyst displayed better onset potential and higher catalytic performance for methanol oxidation.

Table 1. Comparison of our work with several reported works on electrocatalytic activity for methanol oxidation.

Electrocatalyst	Onset potentials (V)	ECSA (cm^2 mg^{-1}Pt)	Current density	Ref
rGO/PEDOT : PSS	-	-	37.5 mA/cm^2	[39]
Pt/C + PpPDA/TiO_2	-0.42	-	191.0 mA mg^{-1} Pt	[40]
Pt-Ag/SnO_2-C	-0.40	75	0.21 mA cm^{-2}	[41]
Pt black	-0.65	124.8	83.6 mA mg^{-1} Pt	This work
Commercial Pt/C	-0.60	147.1	107.3 mA mg^{-1} Pt	
Pt/Ni-Fe LDH	-0.68	153.7	119.2 mA mg^{-1} Pt	
Pt/IL/Ni-Fe LDH	-0.70	203.9	205.6 mA mg^{-1} Pt	

The long-term stability is another important index to evaluate the catalytic performance of an electrocatalyst. By using Amperometric i-t method in the 1.0 M NaOH solution containing 1.0 M CH_3OH, we can characterize the electrocatalyst long-term stability. As shown in Figure 7A, all electrocatalyst show a current density decline in the initial period, perhaps resulting from electrocatalyst poisoning by chemisorbed carbonaceous species formed during the methanol oxidation[42]. At the end, methanol oxidation realize as ready-state, as shown in Figure 7, the current density generate from Pt/IL/Ni-Fe LDH electrocatalyst was higher than other electrocatalysts, indicates that Pt/IL/Ni-Fe LDH electrocatalyst possess the best long-term stability.

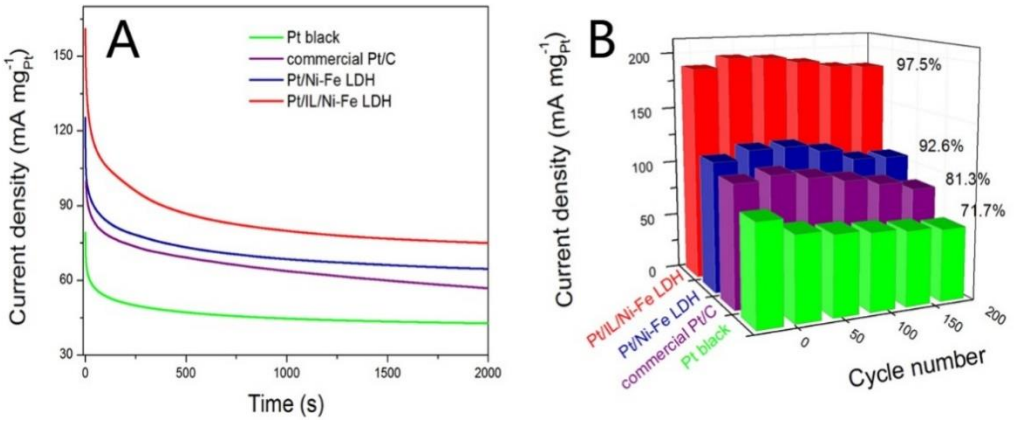

Figure 7. (A) Amperometric i-t curves of Pt black, commercial Pt/C, Pt/Ni-Fe LDH and Pt/IL/Ni-Fe LDH electrocatalyst in 1.0 M CH_3OH containing 1.0 M NaOH at -0.25 V for 2000 s. (B) The peak current density of methanol oxidation in the forward scan on Pt black, commercial Pt/C, Pt/Ni-Fe LDH and Pt/IL/Ni-Fe LDH electrocatalyst vs. the CV cycle number.

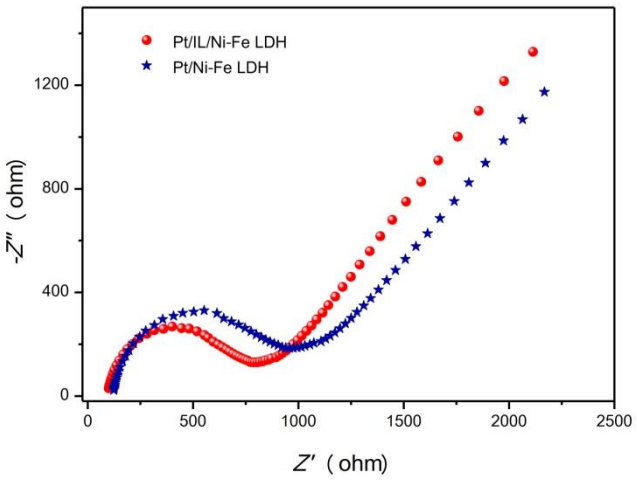

Figure 8. EIS plots of Pt/Ni-Fe LDH and Pt/IL/Ni-Fe LDH electrocatalyst in the solution of 0.1 M KCl containing 5.0 mM $Fe(CN)_6^{3-}/Fe(CN)_6^{4-}$.

Then, we performed 200 cycles CVs to investigate the durability of the electrocatalyst toward methanol oxidation reaction. As we can see from Figure 7B, when the scanning number increase, the peak current density degenerate. That could be ascribed to the generation of intermediates and poisoning

of electrocatalyst during the reaction process, even the reunion desorption of Pt NPs from the substrate. The peak current density after 200 th cycle is about 71.7%, 81.3%, 92.6% and 97.5% of that measured at the first cycle for Pt black, commercial Pt/C, Pt/Ni-Fe LDH and Pt/IL/Ni-Fe LDH electrocatalyst, respectively. It can be seen that the diminish of the electrocatalytic activity for Pt/IL/Ni-Fe LDH is lower than those of Pt and Pt/Ni-Fe LDH electrocatalyst, which further indicating that the present Pt/IL/Ni-Fe LDH having good stability.

Electrochemical impedance spectroscopy (EIS) is a useful technique to characterize the electrocatalytic performance of the electrocatalyst. Figure 8 shows the EIS plots of Pt/Ni-Fe LDH and Pt/IL/Ni-Fe LDH in the solution of 0.1 M KCl containing 5.0 mM $Fe(CN)_6^{3-}/Fe(CN)_6^{4-}$. The size of the arc can be used to estimate the charge transfer resistance of the electrocatalyst during the reaction [43]. As we can see from the Nyquistplots of EIS, the arc radius for Pt/IL/Ni-Fe LDH electrocatalyst are much smaller than that of Pt/Ni-Fe LDH, demonstrates that the combination of IL can conduce to materials conductivity improving and the methanol electro-oxidation rate on Pt/IL/Ni-Fe LDH is much faster than that of Pt/Ni-Fe LDH.

4. CONCLUSIONS

In summary, we synthesized the Pt/Ni-Fe LDH and Pt/IL/Ni-Fe LDH electrocatalyst by a two-step facile process. Firstly, the ultrathin nanoplates of Ni-Fe LDH structure were synthesized, and then Pt NPs was loaded on Ni-Fe LDH that can form highly active electrocatalyst for methanol oxidation reaction in alkaline media. The resulting Pt/Ni-Fe LDH and Pt/IL/Ni-Fe LDH electrocatalyst exhibits higher electrocatalytic activity (with a peak current density of 119.2 mA mg^{-1}_{Pt} and 205.6 mA mg^{-1}_{Pt}), better anti-poisoning ability (I_f/I_b= 5.32 and 5.67) and stability for methanol oxidation compared to pure Pt black electrocatalyst (83.6 mA mg^{-1}_{Pt}, I_f/I_b= 4.98) and commercial Pt/C (107.3 mA mg^{-1}_{Pt}, I_f/I_b= 5.09). In addition, the Pt NPs mean diameter loading on Pt/Ni-Fe LDH and Pt/IL/Ni-Fe LDH electrocatalyst is 4.36 and 3.09 nm, much smaller than that on Pt black and commercial Pt/C electrocatalyst (8.70 nm and 6.48 nm). This study implies that the prepared electrocatalyst has great potential applications in DMFCs.

ACKNOWLEDGMENTS
This work was supported by the National Natural Science Foundation of China (21405086).

References

1. S.S. Munjewar, S.B. Thombre, *Renew. Energy*, 138 (2019) 272-283.
2. W.F. Xie, F.F. Zhang, Z.H. Wang, M. Yang, J.F. Xia, R.J. Gui, Y.Z. Xia, *J. Electroanal. Chem.,* 761 (2016) 55-61.
3. Y. Kin, K. Saito, H. Oda, T. Ando, K. Nakagawa, *Catal. Lett.*, 149 (2019) 1-6.
4. F.F. Zhang, Z.Y. Wang, K.Q. Xu, J.F. Xia, Q.Y. Liu, Z.H. Wang, *Int. J. Hydrog. Energy*, 43 (2018) 16302-16310.
5. S. Eris, Z. Dasdelen, F. Sen, *J. Colloid Interface Sci.*, 513 (2018) 767-773.
6. A.A. Permyakova, B.H. Han, J.O. Jensen, N.J. Bjerrum, Y. Shao-Horn, *J. Phys. Chem. C*, 119 (2015) 8023-8031.
7. D.Y. Chung, K.J. Lee, Y.E. Sung, *J. Phy.s Chem. C*, 120 (2016) 9028-9035.
8. E. Antolini, *Appl. Catal. B-Environ.*, 237 (2018) 491-503.

9. S.H. Yang, F.F. Zhang, Z.H. Wang, Q.L. Liang, *Biosens. Bioelectron.*, 112 (2018) 186-192.
10. Y. Yuan, X.Z. Xu, J.F. Xia, F.F. Zhang, Z.H. Wang, Q.Y. Liu, *Microchim. Acta*, 186 (2019).
11. Z. Xu, X. Lyu, B. Yang, W. Cao, R. Li, X. Zhang, X. Zhang, G. Fan, X. Kong, Q. Liu, *Colloid Surf. A-Physicochem. Eng.,* 569 (2019) 28-34.
12. H. Liu, Y.N. Ding, B.C. Yang, Z.X. Liu, Q.Y. Liu, X. Zhang, *Sens. Actuator B-Chem.*, 271 (2018) 336-345.
13. S.M. Lian, L.N. Gao, M.M. Chen, Z.X. Liu, J. Qiu, X. Zhang, X.L. Luo, R.C. Zeng, Q.Y. Liu, *Appl. Organomet. Chem.*, 33 (2019).
14. K.L. Wu, X. Zhao, M.M. Chen, H.W. Zhang, Z.X. Liu, X. Zhang, X.X. Zhu, Q.Y. Liu, *New J. Chem.*, 42 (2018) 9578-9587.
15. J.P. Liu, Y.Y. Li, X.T. Huang, G.Y. Li, Z.K. Li, *Adv. Funct. Mater.*, 18 (2008) 1448-1458.
16. B.B. Wu, S.L. Zhang, F. Yao, R.J. Huo, F.Z. Zhang, S.L. Xu, *J. Colloid Interf Sci.*, 462 (2016) 183-190.
17. D.C. Carvalho, N.A. Ferreira, J.M. Filho, O.P. Ferreira, J.M. Soares, A.C. Oliveira, *Catal. Today*, 250 (2015) 155-165.
18. J.W. Zhao, J. Chen, S.M. Xu, M.F. Shao, Q. Zhang, F. Wei, J. Ma, M. Wei, D.G. Evans, X. Duan, *Adv. Funct. Mater.*, 24 (2014) 2938-2946.
19. M.F. Shao, F.Y. Ning, J.W. Zhao, M. Wei, D.G. Evans, X. Duan, *Adv. Funct. Mater.*, 23 (2013) 3513-3518.
20. J.W. Zhao, M.F. Shao, D.P. Yan, S.T. Zhang, Z.Z. Lu, Z.X. Li, X.Z. Cao, B.Y. Wang, M. Wei, D.G. Evans, X. Duan, *J. Mater. Chem. A*, 1 (2013) 5840-5846.
21. G.D. Shi, C. Yu, Z.X. Fan, J.B. Li, M.J. Yuan, *ACS Appl. Mater. Interfaces*, 11 (2019) 2662-2669.
22. O. Rahmanian, M. Dinari, M.K. Abdolmaleki, *Appl. Surf. Sci.*, 428 (2018) 272-279.
23. Z.Y. Zhang, D.J. Sun, G.R. Li, B. Zhang, B. Zhang, S.M. Qiu, Y.J. Li, T. Wu, *Colloid Surf. A-Physicochem. Eng.,* 565 (2019) 143-153.
24. B. Zhang, R.T. Hu, D.J. Sun, T. Wu, Y.J. Li, *J. Chem. Eng. Data*, 63 (2018) 4689-4702.
25. H.L. Shi, R.Y. Wang, M.R. Lou, D. Jia, Y. Guo, X.C. Wang, Y.D. Huang, Z.P. Sun, T. Wang, L.X. Wang, *Electrochim. Acta*, 294 (2019) 93-101.
26. L. Luo, Z. Zhou, Y. Ren, G.X. Chen, Q.F. Li, Rsc Adv, 6 (2016) 82726-82732.
27. J. Lou, Y.X. Lu, T.R. Zhan, Y.Q. Guo, W. Sun, C.X. Ruan, *Ionics*, 20 (2014) 1471-1479.
28. Z.Y. Wang, F.F. Zhang, H.Y. Zou, Y.H. Yuan, H.Y. Wang, J.F. Xia, Z.H. Wang, *J. Electroanal. Chem.*, 818 (2018) 198-203.
29. Y.F. Han, Z.H. Liu, Z.P. Yang, Z.L. Wang, X.H. Tang, T. Wang, L.H. Fan, K. Ooi, *Chem. Mater.*, 20 (2008) 360-363.
30. X. Wang, S. Zhou, W.Y. Xing, B. Yu, X.M. Feng, L. Song, Y. Hu, *J. Mater. Chem. A*, 1 (2013) 4383-4390.
31. Y.C. Zhang, F.Z. Zhang, Y.L. Lu, T.T. Chen, L. Yang, *J. Phys. Chem. Solids*, 71 (2010) 604-607.
32. J. Zhang, X.L. Xie, C.J. Li, H. Wang, L.J. Wang, Rsc Adv, 5 (2015) 29757-29765.
33. J.Y. Yu, G.L. Fan, Y. Yang, F. Li, *J. Colloid. Interf. Sci.*, 432 (2014) 1-9.
34. S. Aisawa, S. Sasaki, S. Takahashi, H. Hirahara, H. Nakayama, E. Narita, *J. Phys. Chem. Solids*, 67 (2006) 920-925.
35. G.Y. Shi, Z.H. Wang, J.F. Xia, S. Bi, Y. Li, F.F. Zhang, L. Xia, Y.H. Li, Y.Z. Xia, L.H. Xia, *Electrochim. Acta*, 142 (2014) 167-172.
36. M.S. Wietecha, J. Zhu, G.H. Gao, N. Wang, H. Feng, M.L. Gorring, M.L. Kasner, S.F. Hou, *J. Power Sources*, 198 (2012) 30-35.
37. Z.H. Wang, W.F. Xie, F.F. Zhang, J.F. Xia, S.D. Gong, Y.Z. Xia, *Electrochim. Acta*, 192 (2016) 400-406.
38. Y.J. Wang, J.K. Wang, G.K. Han, C.Y. Du, Y.R. Sun, L. Du, M.C. An, G.P. Yin, Y.Z. Gao, Y. Song, *Appl. Surf. Sci.*, 473 (2019) 943-950.
39. B. Baruah, A. Kumar, *Electroanalysis,* 30 (2018) 2131-2144.

40. H. Rostami, A.A. Rostami, A. Omrani, *Electrochim. Acta*, 191 (2016) 536-547.
41. B. Ruiz-Camacho, A. Medina-Ramirez, R. Fuentes-Ramirez, C.M. Gomez, *J. Solid State Electrochem.*, 21 (2017) 2449-2456.
42. Z.Q. Gao, M.M. Li, J.Y. Wang, J.X. Zhu, X.M. Zhao, H.J. Huang, J.F. Zhang, Y.P. Wu, Y.S. Fu, X. Wang, *Carbon*, 139 (2018) 369-377.
43. J.F. Xia, X.Y. Cao, Z.H. Wang, M. Yang, F.F. Zhang, B. Lu, F. Li, L. Xia, Y.H. Li, Y.Z. Xia, *Sens. Actuator B-Chem.*, 225 (2016) 305-311.